Covariance analysis tool for far non-cooperative rendezvous: Application to mission profile and sensor suite with ISS-like target

Leonore de Mijolla, Bruno Cavrois*, Alexandre Profizi*, Cédric Renault**, and Alexander Cropp****
**EADS Astrium SAS – Space Transportation*
51-61 Route de Verneuil, 78130 Les Mureaux, France
***EADS Astrium SAS – Space Transportation*
Rue du Général Niox, 33165 Saint Médard en Jalles, France
****European Space Agency – ESTEC*
Noordwijck, Netherlands

Abstract
Non-cooperative rendezvous is a key aspect of space debris removal, which will be very important in the next decades as the number of orbiting objects keeps on growing rapidly. In this paper, emphasis is placed on navigation concerns during non-cooperative far rendezvous. Navigation performances are limited in case of angles-only navigation by the fact that the chaser/target range is not observed. One solution, based on additional manoeuvres dedicated to observability issues, is explored. A covariance analysis tool has been developed in order to analyze the impacts of thrust manoeuvres and sensor suite performance. Sensitivity analyses compare the performances in various cases from a realistic rendezvous configuration with ISS-like target.

1. Introduction

1.1 Overview

Non-cooperative rendezvous is a challenging phase of space debris removal, which may become critical in the next decades as the number of orbiting objects keeps on growing rapidly. Orbital non-cooperative rendezvous consists in a series of orbital manoeuvres and controlled trajectories, which successively bring the active vehicle ("the chaser") into the vicinity of the passive vehicle ("the target"). As a first step of debris removal, non-cooperative rendezvous with the International Space Station (ISS) is under study. Presented in this paper, the activity has been performed in the frame of the Versatile Autonomous Concept (VAC) Phase A/B1, held by Astrium under ESA contract in 2011/2012. The VAC project has the purpose to evolve the ATV toward a modular space tug concept, with emphasis on new technologies (e.g. RdV to unprepared targets) and transportation system versatility (to allow multiple application scenarios). The current technology implemented on the Automated Transfer Vehicle (ATV), developed by ESA, EADS Astrium, and their partners, three times flight-proven, consists in cooperative rendezvous based on targets specifically mounted on the ISS [1]. Cooperative modes implemented in ATV rely on a proximity link between both vehicles providing relative GPS data and attitude data from ISS.

In the frame of non-cooperative rendezvous, the suite of sensors is revisited versus cooperative rendezvous standards. The case of angles-only navigation is studied. It concerns the basic case of sensor suite composed of IMU, star tracker, and camera. If only LoS measurements are performed, the relative position and velocity is not completely observable. The trajectory can be estimated up to a homothetic factor. Two solutions can be investigated. The first solution removes the limitation by introducing direct range measurements. Two sensors have the capability to provide such measurements: LiDAR and camera with image processing based on the apparent diameter of the target. Its limitations are numerous, especially at far distance, where camera accuracy is limited and LiDAR is not working at distance above 3-km. Moreover, the target is not necessarily well known and can be spinning. Consequently, direct range measurements from camera could be hardly performed. A second solution is based on performing manoeuvres under few conditions. It allows theoretically a complete observation of the relative

dynamics. Nevertheless, the ability to observe the manoeuvres depends on the characteristics of the accelerometers and camera measurements.

The paper focuses on the latter solution. From a review on observability issues and mission requirements, several trajectories are elaborated. A covariance analysis tool has been developed to test them. This tool can predict navigation error like usual Monte-Carlo tool in a single run. Its objective is three-fold: 1) improvement of knowledge of observability issues by introducing the knowledge of performed manoeuvres and the camera characteristics 2) assessment of interest of sensor defects estimation; 3) analysis of the performances of various sensor suites. Similar tools have been presented in the following papers:

- J.r. Yim introduces absolute dynamics and position/velocity estimation of spacecraft in a tool allowing only LoS measurements [2].
- S-G. Kim bases its tool on estimation of relative attitude, position and gyro biases [3].
- Whereas D. Woffinden's tool deals with absolute navigation and complex sensors models adding star tracker measurements, it does not include the accelerometers errors [4].
- In the most recent developed simulator, J. Schmidt implements accelerometer errors but does not estimate attitude errors [5].

Thus, the covariance analysis tool presented and used hereafter enables estimation as well as the relative position and velocity errors, the absolute chaser attitude error, and the main sensor defects (IMU, star tracker, camera and LiDAR).

After review on observability issues and study of trajectory designs in Section 2, the capabilities of the covariance analysis tool are presented in Section 3. Section 4 contains several applications of the covariance analysis. A summary of results and concluding remarks are given in the last section.

1.2 Coordinate frames and notations

Abbreviations

ATV	**A**utomated **T**ransfer **V**ehicle
IMU	**I**nertial **M**easurement **U**nit
ISS	**I**nternational **S**pace **S**tation
LoS	**L**ine **o**f **S**ight
STD	**St**andard **D**eviation
VAC	**V**ersatile **A**utonomous **C**oncept
w.r.t.	**w**ith **r**egard **t**o

Coordinate frames

The inertial frame (i) has its origin at the centre of the Earth and axes are non-rotating w.r.t. to fixed stars. (O_i, x^i, y^i, z^i) defines the frame. z^i axis is coincident with the Earth polar axis.
The Local Vertical Local Horizontal frame (LVLH) is linked to the trajectory of the target. z^{LVLH} axis points toward the Earth (local vertical), x^{LVLH} axis is in the velocity frame, orthogonal to z^{LVLH} axis, and finally y^{LVLH} axis completes the orthogonal frame.

The chaser frame (O_c, x^c, y^c, z^c) is positioned w.r.t. a mechanical frame. x^c axis is the chaser longitudinal axis.
The camera frame (cam) and the star tracker frame are the frame linked to the sensors. These frames are fixed w.r.t. chaser frame. The assumptions that these frames are identical to the chaser frame are made in this paper without loss of generality.
Figure 1 illustrates the three main frames.

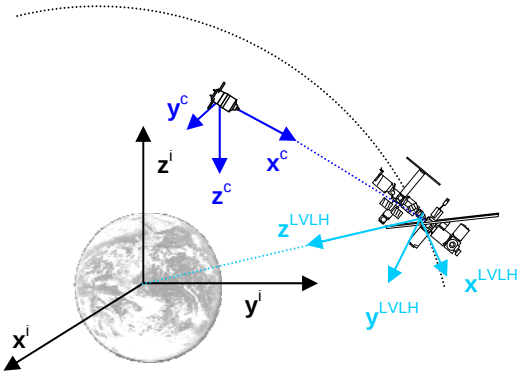

Figure 1: Illustration of inertial frame, LVLH frame, and chaser frame

Nomenclature

Parameters		Superscripts	
t	Time	o^c	Chaser body frame
X	State vector	o^{LVLH}	Local Vertical Local Horizontal frame
$r\ (x \quad y \quad z)$	Position	o^{cam}	Camera frame
$v\ (vx \quad vy \quad vz)$	Velocity	o^{st}	Star tracker frame
γ	Acceleration	o^i	Inertial frame
θ	Attitude		
E	Defects vector	Subscripts	
ε	Misalignments	o_c	Chaser
δo	Standard deviation	o_{gyro}	Gyrometer
		o_{acc}	Accelerometer
		o_{st}	Star tracker
		o_{cam}	Camera

Note that all values and figures are 1-sigma in this paper.

2. Relative state observability and trajectory design for non-cooperative rendezvous

2.1 Preliminary statements on observability

Observability concerns are a key subject during orbital rendezvous. Indeed, the capability to estimate relative position and velocity between chaser and target vehicles is limited in case of angles-only navigation. Navigation with LoS-only measurements is subject to ambiguity: only the ratio between range and velocity can be observed. This ratio is called 'homothetic factor'. Figure 2 illustrates three kinds of relative trajectories of the chaser with respect to the target: V-bar station keeping, circular orbit, football orbit. In each case, the blue and red chasers observe the same evolution of LoS measurements along time.

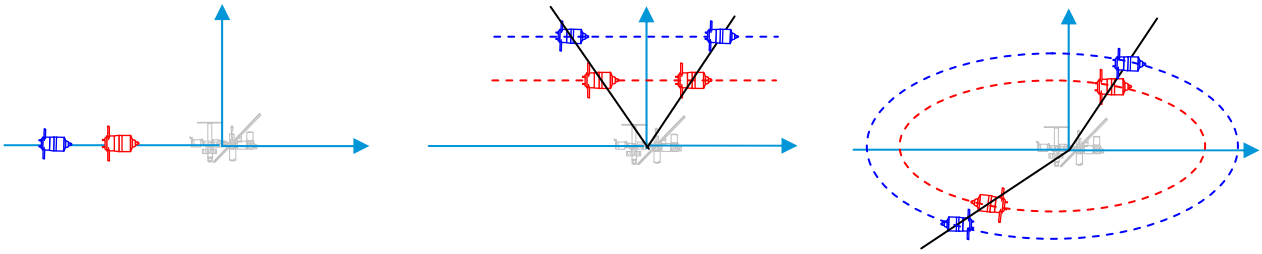

Figure 2: Illustration of non-observable family of orbits in LVLH frame

Nevertheless, LoS measurements remain important since the most accurate parameter on position/velocity improves the knowledge on the other parameters. Easily demonstrated thanks to the Clohessy-Wiltshire equations, Figure 3 shows geometrically this statement.

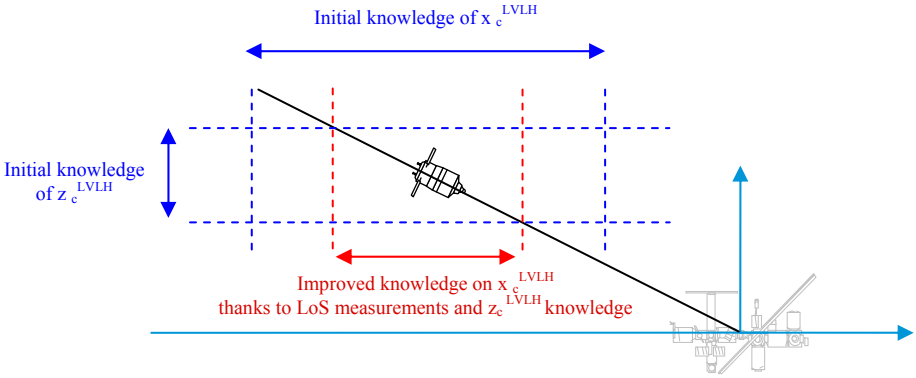

Figure 3: Improvement provided by LoS measurements without manoeuvre in LVLH frame

As a consequence, when a measurement is performed, the navigation errors are proportional to the state:

$$\text{At } t = t_{LOS\ measurments},\ \begin{bmatrix} \delta x_c^{LVLH} \\ \delta y_c^{LVLH} \\ \delta z_c^{LVLH} \\ \delta Vx_c^{LVLH} \\ \delta Vy_c^{LVLH} \\ \delta Vz_c^{LVLH} \end{bmatrix} = \alpha * \begin{bmatrix} x_c^{LVLH} \\ y_c^{LVLH} \\ z_c^{LVLH} \\ Vx_c^{LVLH} \\ Vy_c^{LVLH} \\ Vz_c^{LVLH} \end{bmatrix} \quad \textbf{(1)}$$

$$\text{With } \alpha = \min\left(\frac{\delta x_c^{LVLH}}{x_c^{LVLH}}, \frac{\delta y_c^{LVLH}}{y_c^{LVLH}}, \frac{\delta z_c^{LVLH}}{z_c^{LVLH}}, \frac{\delta Vx_c^{LVLH}}{Vx_c^{LVLH}}, \frac{\delta Vy_c^{LVLH}}{Vy_c^{LVLH}}, \frac{\delta Vz_c^{LVLH}}{Vz_c^{LVLH}} \right), \text{ the homothetic factor.} \quad \textbf{(2)}$$

Angles-only navigation performance can be improved when manoeuvres are performed thanks to an *a priori* knowledge (propulsion model) or measurement of the acceleration (accelerometers) and a change in the measurement profile. Requirements on the manoeuvres have been detailed in literature [4]. The performed manoeuvre direction has to guarantee a unique measurement profile, i.e. a change in the LoS vector. Consequently, the manoeuvre has to follow one of these conditions. The manoeuvre can be performed in any direction when the chaser is not moving on the LoS direction. If the chaser is moving on the LoS direction, the manoeuvre has to be either parallel to the range vector in the opposite direction (typically, the chaser passes beyond the target) or not parallel to the LoS vector.

In the theoretical case, the boost and camera characteristics are perfectly known. Then, since manoeuvre is performed, the observability is established. In a more realistic case, on the one hand, the boost is not perfectly known due to the propulsion model or the IMU defects, and on the other hand, the camera measurement performances are reduced due to camera misalignments and camera noise.

The ambiguity remains due to the uncertainty on the acceleration and to the linearity (at first order) of the target-chaser relative movement equations. Indeed, even if the manoeuvres modifying the LoS profile are not sufficiently

known, they do not improve the observability of the relative state. On Figure 4, the blue and the red chasers observe the same evolution of LoS measurements along time if the boosts performed by the red chaser are larger than the blue chaser boosts (2 times larger if its initial distance to the target is 2 times larger).

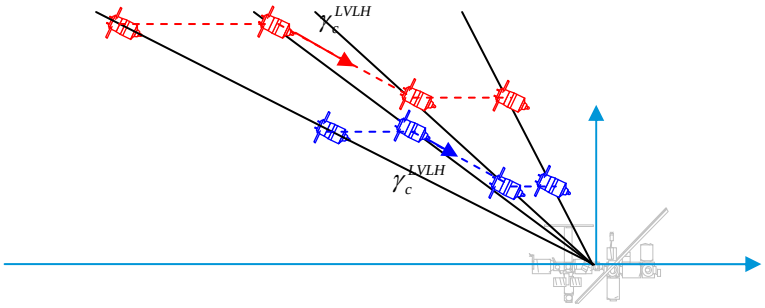

Figure 4: Illustration of unobservable orbit due to partially known manoeuvre in LVLH frame

Similar statements can be established on camera defects. Figure 5 illustrates the limitation of detectability due to camera defects. At t_1, the range is not observed. A manoeuvre perfectly known is performed. The observability angle θ is defined as the LoS angle introduced by the manoeuvre. At t_2, the range is estimated. The sensor accuracy ε_{cam} and the observability angle θ_{obs} drive the uncertainty δr on the relative range.

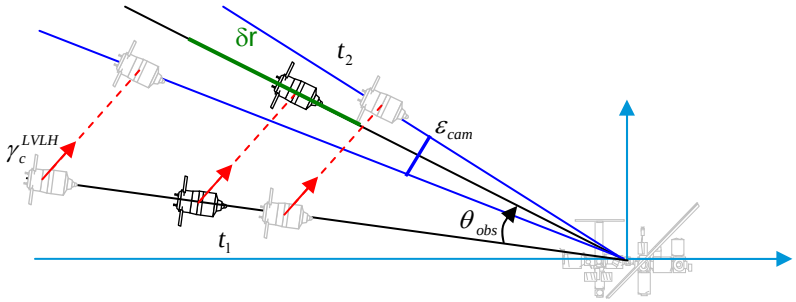

Figure 5: Illustration of limitation of observability due to camera misalignments

2.2 Reference Mission

The design of rendezvous phase is a tricky issue since it depends on numerous parameters: sensors suite, navigation architecture, overall duration, propellant consumption, thermal constraints, and safety constraints relative to the target. The reference mission studied in this paper is close to the ATV one [6]. The chaser approaches the target along the orbital velocity direction. The far rendezvous is commonly divided in three main sub-phases:

- At initialization S_0, the chaser is located on circular orbit slightly lower than the ISS one. The navigation is initialized thanks to absolute navigation means: GPS measurements and target ephemerides. The camera acquisition and navigation convergence are processed. This first phase is called “pre-homing” and ends with the first manoeuvre occurring at S_1.

- Then, the “homing phase” takes place from S_1 to S_2. The hold point S_2 has to be set few kilometres before continuing on rendezvous. This hold point or free drift phase allows the wait for ground decision. This hold point can also be used for LiDAR acquisition and navigation filter convergence. It is basically set to 3km.

- The “closing phase” designs the achievement of S_3, at 300 m.

The rendezvous mission continues with the close rendezvous.

The chaser’s attitude is constrained by pointing on the target during the rendezvous in order to keep the latter in the camera and LiDAR field-of-views.

In addition, the rendezvous with ISS-like target is strongly constrained by safety issues. Two forbidden areas are defined and have to be avoided in case of GNC failure (= Safe free drift trajectory):

- Approach Ellipsoid – A zone around the ISS with the following dimensions: ellipsoid of 4km x 2km x 2km, centred at the ISS centre of mass, with the major axis along the x^{LVLH} axis.

- Keep Out Sphere – A safety sphere centred on the ISS centre of mass, with a radius of 200m and which shall be entered only following predefined corridors and upon receipt of due authorization at the end of the closing phase.

As base of non-cooperative rendezvous studies, Figure 7 illustrates the reference trajectory. This trajectory takes into account all safety constraints required for ISS rendezvous. Initial differential altitude is set to 2.5km.

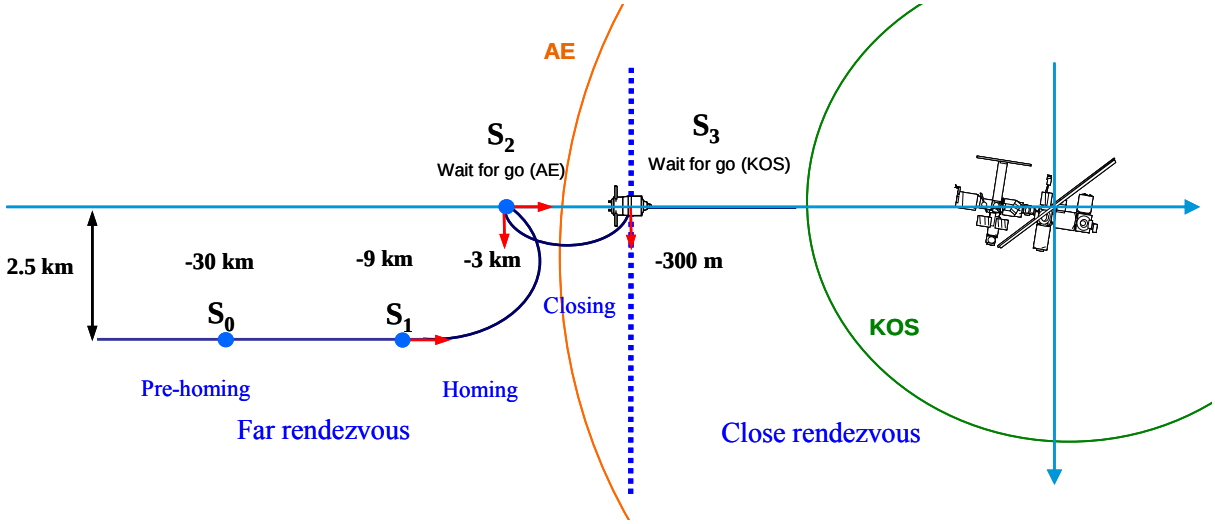

Figure 7: Reference mission profile in LVLH frame

2.3 Trajectory design

According to the previous statements, four trajectories are elaborated thanks to an in-house tool in order to determine: 1/ if the mission profile influences the navigation performance; 2/ If anticipation of manoeuvres can improve the navigation performance. This mission analysis optimisation tool can simulate Keplerian orbit and several perturbations (various gravity models, solar pressure, drag, third body Moon/Sun…). No J2 gravity model and additional disturbance is implemented in the reference case. Indeed, differential drag between ISS and chaser results in differential non-gravitational acceleration to chaser on x^{LVLH}. A worst case can lead a constant $10^{-5} m/s^2$ acceleration. This disturbance is not included in the reference trajectory and can be dealt as an additional residual low accelerometer bias ($1\mu g$ for drag to be compared to $5\mu g$ for accelerometer bias). The trajectories are described hereafter and are shown in Figure 8:

- 5km-initial altitude trajectory – This trajectory studies the sensitivity to initial altitude. The 5-km initial altitude is similar to ATV one. Thus, this case illustrates current flight mission and assesses its advantage to reuse. This initial constraint of 5-km altitude deals with ISS safety constraints and limitation of drift during pre-homing phase.

- Trajectory with small observability manoeuvre – A manoeuvre is performed with the only objective to improve observability before S_1. This trajectory simulates a 1-km lateral move resulting from 300-s boost. With the considered initial altitude, the manoeuvre duration does not allow a complete period of orbit. That is why the stop boost is performed as soon as the position on y^{LVLH} is null again. With a 1.13-m/s boost magnitude, this move has the same order of magnitude than the actual ATV manoeuvres. The end of mission is similar to the reference trajectory.

- Trajectory with high observability manoeuvre – Higher than the previous trajectory, a 2-km lateral move is performed before S_1 ($\Delta V \sim 2.26$m/s with a 600-s boost).

- Minimum manoeuvre trajectory – This trajectory minimizes the number of manoeuvres. Only two thrusts are performed from 3km. This trajectory does not satisfy all safety requirements. However, it helps comparison for rendezvous with debris where only one hold point could be needed.

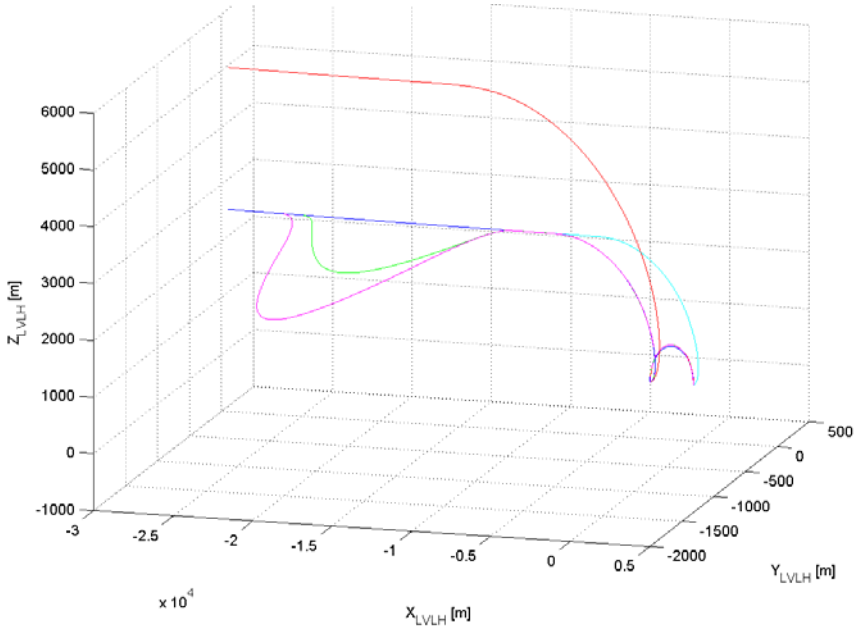

Figure 8: Rendezvous trajectories in LVLH frame. The reference trajectory is in dark blue, similar to light blue before 8 km and, close to the pink line below 8 km.

3. Covariance analysis tool

The covariance analysis tool for far rendezvous is based on the linearization of navigation algorithms for non-cooperative orbital rendezvous. This navigation analysis tool is quicker and more flexible than a Monte-Carlo tool. The tool is capable of estimating navigation state STDS in different case scenarios and allows multiple analyses of navigation performance in far rendezvous. Some examples are:

- Evaluate impacts of sensor performance by sensitivity studies.
- Evaluate impacts of measure schedules and performance.
- Evaluate impacts of different trajectory profiles
- Analysing and selecting the state parameters to be included in on-board systems. The functionality to reduce the state vector is included in the tool. It implies that some parameters are not estimated by the filter, however their effects in terms of navigation errors are present in the system and do affect propagation dynamics.

To satisfy these needs, the covariance analysis tool has been developed in Matlab. It can be easily modified, which corresponds to our requirements in terms of flexibility and speed.

The covariance analysis tool is based on a 42-state extended Kalman filter producing the error covariance matrix along trajectory. The state vector used for the propagation of the covariance includes all the modelled errors that have a first or second order impact on the navigation accuracy during the rendezvous:

$$X = \left[\delta r_c^{LVLH} \quad \delta v_c^{LVLH} \quad \delta\theta_{c-i}^{c} \quad E_{gyro}^{c} \quad E_{acc}^{c} \quad \varepsilon_{cam}^{cam} \quad \varepsilon_{st}^{st} \quad \varepsilon_{lidar}^{lidar}\right]^T \tag{3}$$

Where,

δr_c^{LVLH}	relative position error w.r.t. target in LVLH
δv_c^{LVLH}	relative velocity error w.r.t. target in LVLH
$\delta\theta_{c-i}^{c}$	attitude error w.r.t. the inertial frame in chaser frame
E_{gyro}^{c}	gyro flaws in chaser frame including drift, scale factor, and misalignments
E_{acc}^{c}	accelerometric flaws in chaser frame including bias, scale factor, and misalignments
ε_{cam}^{cam}	misalignment of the visible camera in camera frame
ε_{st}^{st}	misalignment of the star tracker in star tracker frame
$\varepsilon_{lidar}^{lidar}$	misalignment of LiDAR in LiDAR frame

The dynamics are modelled by the Clohessy-Wiltshire equations which are adapted to the space rendezvous mechanics. Contrary to the classical dynamics equations, the Clohessy-Wiltshire equations work directly on the relative position/velocity between chaser and target in the LVLH frame. This method reduces the computation load by reduction of the state parameters since classical dynamics equations imply the estimation of chaser and target position/velocity/attitude separately. These equations are derived from several assumptions:

- Orbital perturbations (high order gravitational terms, atmospheric drag, solar radial pressure, lunar attraction …) are neglected,
- Distance between target and chaser should be small w.r.t. Earth distance,
- No commanded thrust is performed on the target,
- The target moves on a circular orbit.

A camera, star tracker, and LiDAR measurement models are implemented in the tool. As mean of absolute navigation, the star tracker provides absolute attitude data in inertial frame. The camera provides azimuth and elevation angles by measuring location of the barycentre in the camera focal plane. An additional measurement with apparent angular diameter of the target can provides information on the range. It requires an *a priori* knowledge of the apparent diameter of the target. Visible and infrared cameras can be configured thanks to specific noise models and measurement frequency.

4. Navigation performances

In this section, the tool is used to assess navigation performances on two sensitivities: sensitivity on trajectories designed in Section 2, and sensitivity on sensor suite. The configuration is set on realistic (according current ATV mission) or expected conditions for non-cooperative rendezvous. The initial uncertainties at S_0 for the position/velocity are relative to the current absolute navigation capabilities (See Table 1).

Table 1: Initial uncertainties on position and velocity

position	Value	velocity	Value
$\delta x_c^{LVLH}(t_0)$ [m]	275	$\delta v_{x_c}^{LVLH}(t_0)$ [m/s]	0.33
$\delta y_c^{LVLH}(t_0)$ [m]	166	$\delta v_{y_c}^{LVLH}(t_0)$ [m/s]	0.33
$\delta z_c^{LVLH}(t_0)$ [m]	166	$\delta v_{z_c}^{LVLH}(t_0)$ [m/s]	0.33

Reference attitude error at S_0 is 0.17° at 1σ. The characteristics of ATV's IMU are retained as a reference:

Accelerometric bias = $8.3\,\mu g$ | Accelerometric scale factor = 10^{-4}

Accelerometric non-orthogonalities [°] = $\begin{bmatrix} 0 & 7.10^{-2} & 7.10^{-2} \\ 0 & 0 & 0 \\ 0 & 7.10^{-2} & 0 \end{bmatrix}$

Gyrometric drift = 1.3 °/h | Gyrometric scale factor = 10^{-4}

Gyrometric misalignments [°] = $\begin{bmatrix} 0 & 7.10^{-2} & 7.10^{-2} \\ 7.10^{-2} & 0 & 7.10^{-2} \\ 7.10^{-2} & 7.10^{-2} & 0 \end{bmatrix}$

The reference sensors suite is made up of IMU, star tracker and infrared camera without direct range measurements. Consequently, reference case refers to angles-only navigation. Their characteristics are described in Table 2.

Table 2: Sensor characteristics

Star tracker	**Value**
Misalignments [°]	0.07
Operational range [m]	from S_0
Noise [arcsec]	18
Camera	
Focal [mm]	56.5
Misalignments [°]	0.17
Operational range [m]	from S_0

LoS measurement noise of camera varies from 0.05° up to 0.6°. Unlike the infrared camera, the visible camera is affected by eclipse periods. Although LiDAR is implemented in the tool, this measure is not used in the following tests.

4.1 Sensitivity on trajectory manoeuvres

Given in Figure 9, acceleration profiles and the estimated position STDs are function of time and position. Indeed, different mission schedules and initialization imply different timelines. On the figures, colours are coherent with the colours of trajectories in Figure 8.

- 5km-initial-altitude trajectory is the shortest one w.r.t. time regarding higher velocity during free drift phase. During the 10 first meters, navigation convergence performances are similar to the reference trajectory in Figure 9 (c). Then, this trajectory differs on acceleration profile (See Figure 9 (a)). With longer boost durations during homing phase, accelero defects increase the position STD. Estimates of star tracker misalignments, camera misalignments, and attitude knowledge are not significantly affected by the initial differential altitude.

- Comparing the trajectories with observability manoeuvre and the reference trajectory between 1000s and 6000s, the position accuracy is not improved by additional manoeuvres. These out-of-plane manoeuvres allow good estimate of star tracker misalignments, camera misalignments, and accelero defects especially on y^{LVLH}. Propagation of IMU errors is major during the accelerated phases. As consequence, the position STDs are superior to the reference ones during pre-homing and homing phases.

  Trajectories with observability manoeuvres are tested in two additional configurations in Figure 10.

  In Figure 10 (a), manoeuvres are perfectly known by IMU without defect. It supports that IMU is in charge of increase of position STDs during the observability manoeuvres. With no IMU errors, the manoeuvres causes a decrease of position STDs on x^{LVLH} and z^{LVLH}. Difference on the position STDs is extensively reduced from the homing phase where manoeuvres are performed on all tested profiles.

  In Figure 10 (b), manoeuvres are still perfectly known and camera noise is strongly reduced (divided by 10). Before the first boost, the homothetic factor ($\delta z^{LVLH} / z^{LVLH} = \delta x^{LVLH} / x^{LVLH}$) is well observable. In this configuration, the moves are well observed by camera. Then, correction of homothetic factor is faster and stronger. Final accuracies are similar in this test.

- Trajectory for debris is different rendezvous mission from previously, boosts occur very lastly and no boost is performed on z^{LVLH} axis. Consequently, accelero defects are less estimated. Nevertheless, the final precision at S_3 is better on debris-like trajectory. The chaser is closer to the target during the second phase. Although the observability angle is higher and the position is better estimated, debris-like trajectory is more risky from a safety point of view for ISS-like target.

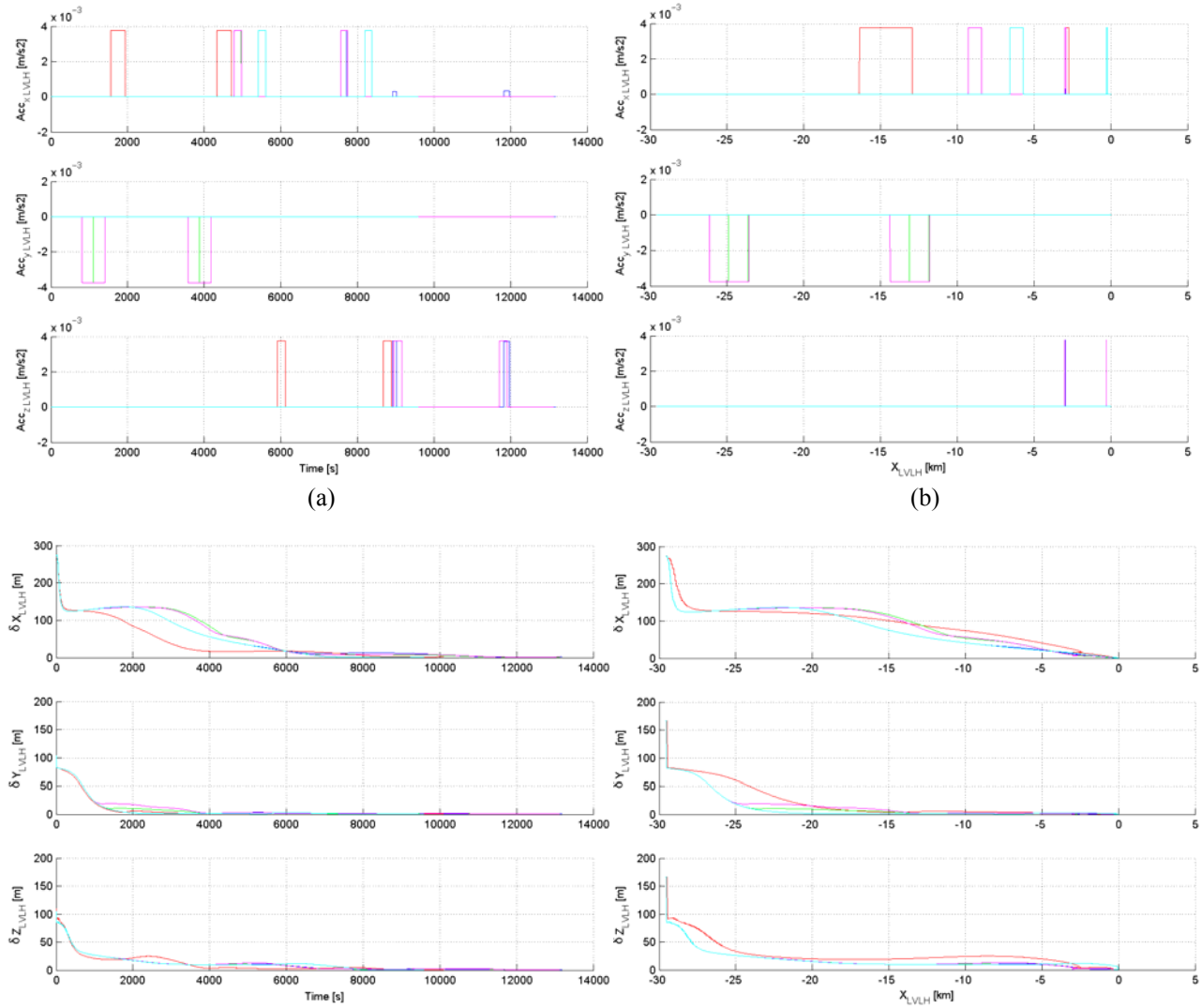

(a) (b)

(c) (d)

Figure 9: Acceleration profile w.r.t. time (a) and w.r.t. range (b),
and position STDs w.r.t. time (c) and w.r.t. range (d) for sensitivity to trajectory.

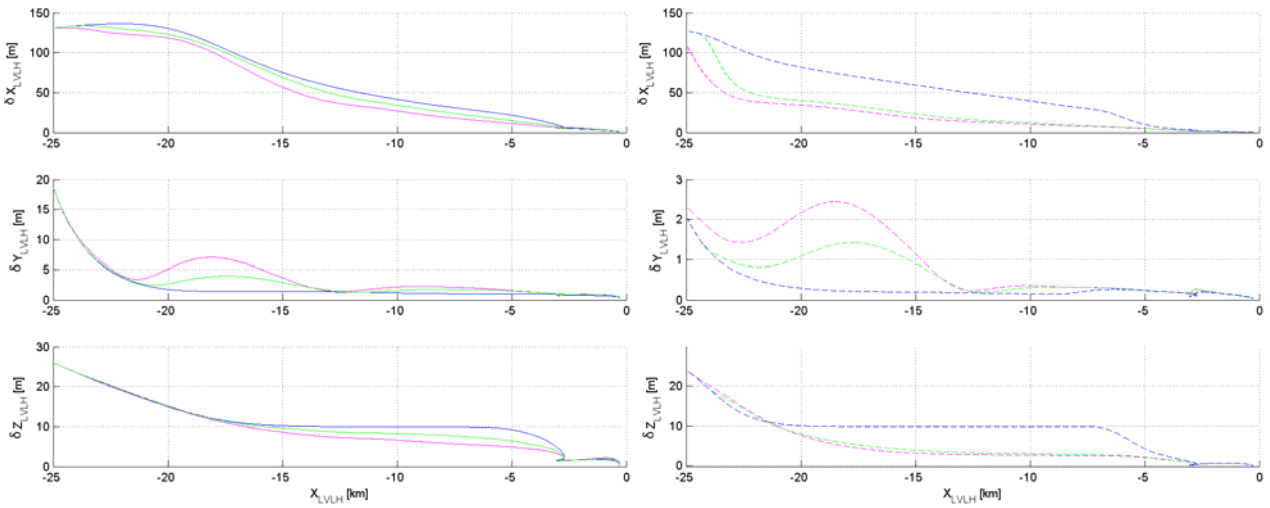

(a) (b)

Figure 10: Position STDs for sensitivity to trajectory with perfect accelerometers (a),
with perfect accelerometers and camera noise divided by 10 (b)

4.2 Sensitivity on sensor suite

Three sensor suites are tested on the reference trajectory (See Table 3). Visible camera and infrared camera do not have the same measurement frequency. The visible camera is affected by the sun eclipses since target is not visible. In this case, a loss of measurement lasting 40 minutes occurs every orbital period. Consequently, from the navigation point of view, an extended 50-minute blackout takes into account sensor re-acquisition and navigation convergence. These blackout periods are illustrated in Figure 11 in a favourable configuration where sun phases occur mainly during the boosts. Nevertheless, measurements are not performed during the second boost of the closing phase.

Figure 12 shows position STD and camera misalignment estimates from S_0 to S_3. From S_0 to S_1, position STDs decrease proportionally to the estimation of camera misalignments. In reference case and Case 1, the star tracker measurements are provided. The estimation of camera misalignments reaches precision of star tracker after convergence. In Case 1, position STDs are strongly correlated with the availability of camera measurements. When eclipse phase occurs at ~8 km, position STDs diverge. In Case 2, star tracker measurements are not available. Camera misalignments cannot take advantage of star tracker precision. Attitude knowledge estimate is also impacted. Consequently, position STDs are ~200 m bigger on x^{LVLH} axis at 15 km without star tracker measurements.

Difference between the various sensor suite performances is noted at S_3. The manoeuvres being not observable, final accuracy is determined by homothetic factor, and so mainly by estimate of camera defects. Thus, the advantage to estimate camera deflect is underlined when star tracker measurements are available.

Table 3: Cases of sensitivity to sensor suite

Sensors suite (enable)	Reference Case	Case 1	Case 2
Visible camera	/	true	/
Infrared camera	true	/	true
Star tracker	true	true	/

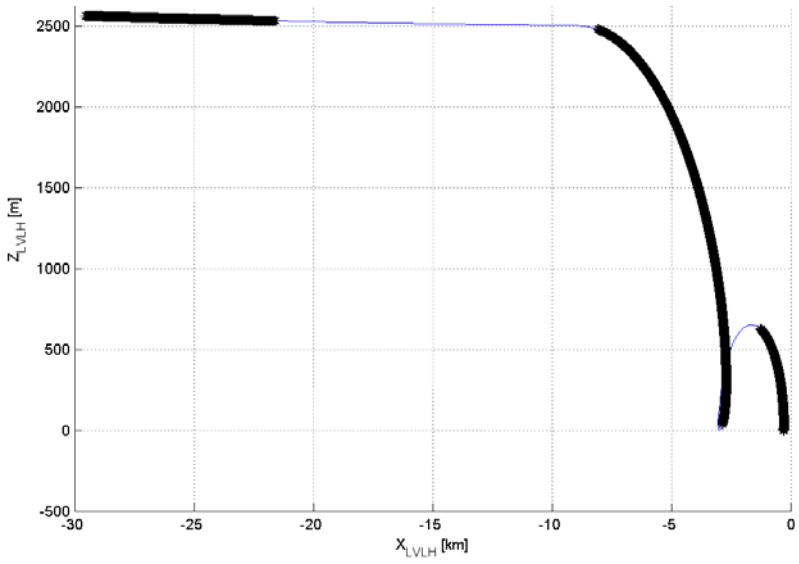

Figure 11: Blackout periods for visible camera measurements with reference trajectory in LVLH frame. The chaser trajectory is blue line. The blackout phases are thick black line.

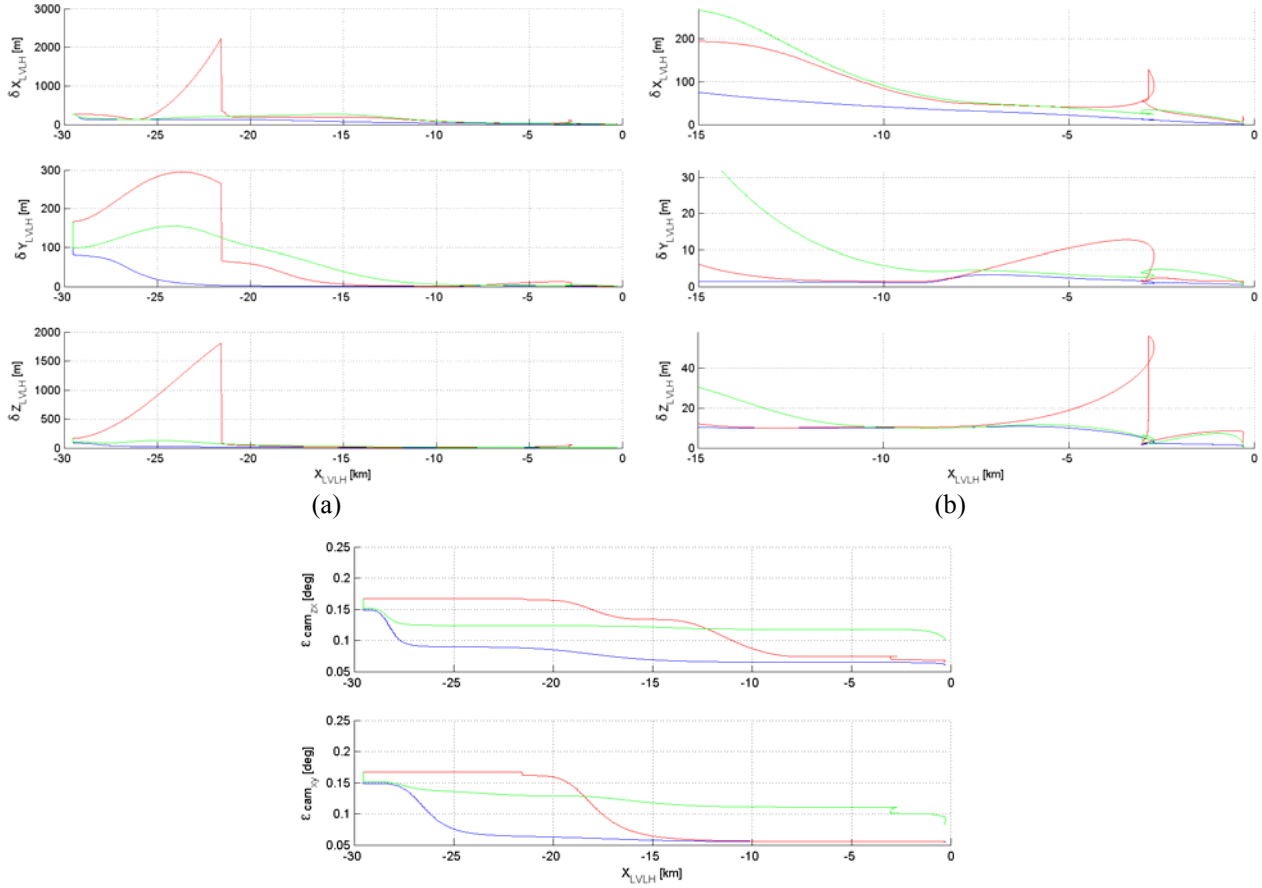

Figure 12: Position STDs (a) and (b), and camera misalignments (c) for sensitivity to sensor suite.

5. Synthesis

This paper has studied the relative navigation issues involved during non-cooperative rendezvous and has focused on an application consisting in non-cooperative rendezvous mission with the ISS. In the frame of the VAC Phase A/B1, a covariance analysis tool including relative dynamic model derived from Clohessy-Wiltshire equations and a large sensor suite has been used in industrial application. The tool provides a fast mean to size a vehicle from the sensors suite to the actuators architecture for any kind of non-cooperative rendezvous scenario (either ISS, repairing or refulling mission or debris removal).

5.1 Summary of results

One solution to remove the limitation of observability during non-cooperative rendezvous is investigated. Performing manoeuvres under few conditions allows theoretically removing the global uncertainty. Nevertheless, the capacity to observe the manoeuvres depends on the characteristics of accelerometers and camera measurements. This statement introduces the idea of degree of observability, function of the previous characteristics and the observability angle introduced by the manoeuvre.
The tool tests two critical sensitivities on angles-only navigation: Sensitivity on trajectory design, and sensitivity on the sensor suite.
Mission for rendezvous with ISS is very constrained mainly due to safety requirements and rendezvous dynamics. Thus, design of trajectory is strongly limited. Results have shown that the reference configuration does not allow good observation of manoeuvres. Besides, opposite effect is noted since position errors growth with accelerated phases propagating IMU errors. In favourable configuration, i.e. minimal accelero defects and camera with good precision, trajectories with out-of-plane manoeuvres are interesting. Nevertheless, the reference trajectory presents initially a large observability angle at the end of the homing phase.
Then, the tool has demonstrated its capability to test various sensor suites. Especially, results show the camera misalignments are estimated by the filter despite the limited accuracy on the full state vector (unobservable states

during the pre-homing phase). The advantage of improving the capability of filter estimation is underlined. Although misalignment estimation does not remove the uncertainty about the position, yet it increases the robustness with respect to attitude error initialisation.

5.2 Further work

Thanks to the covariance analysis tool, a first navigation architecture and sensor architecture could be proposed. In the future, sensors performance models will be improved. Similarly, while the dynamic model is sufficient for the ISS rendezvous, it shall be upgraded to elliptical orbit rendezvous scenario.
In parallel, a Monte-Carlo tool is under development to check the influence of deterministic parameters versus statistical parameters. It will pave the way for a global GNC tool for active debris removal with real time algorithms.

References

[1] Pinard, D., S. Reynaud, P. Delaux. Accurate and Autonomous Navigation for the ATV. EUCASS
[2] Yim J.r. 2004. Autonomous Orbit Navigation of Two Spacecraft System Using Relative Line Of Sight Vector Measurements. Korea Aerospace Research Institute. ASS 04-257.
[3] Kim S-G. Kalman Filtering for Relative Spacecraft Attitude and Position Estimation. University at Buffalo
[4] Woffinden D. 2008. Angles-only navigation for autonomous orbital rendezvous. PhD Thesis. Utah State University.
[5] Schmidt J., D. Geller, F. Chavez. 2009. Improving Angles-Only Navigation Performance by Selecting Sufficiently Accurate Accelerometers. Utah State University, Air Force Research Lab.
[6] Cavrois B., S. Reynaud, G. Personne, S. Chavy, S. Strandmoe. 2009. ATV GNC and safety functions synthesis: overall design, main performances and operations. AIAA-092407.

Acknowledgment

The authors thank the Astrium's team involved in the studies of far non-cooperative rendezvous: Blanca Gonzalez-Font, Jean-François Jourdas, Adrien Chapelle, and Sylvain Roussel.